AMERICAN ACADEMY OF OPHTHALMOLOGY®

Retinal Microvasculature Causally Affects the Brain Cortical Structure: A Mendelian Randomization Study

Xiaoyue Wei, PhD,[1,2,*] *Wai Cheng Iao, MBBS,*[1,2,*] *Yi Zhang, MBBS,*[3] *Zijie Lin, MBBS,*[3] *Haotian Lin, PhD*[1,2,4]

Purpose: To reveal the causality between retinal vascular density (VD), fractal dimension (FD), and brain cortex structure using Mendelian randomization (MR).

Design: Cross-sectional study.

Participants: Genome-wide association studies of VD and FD involving 54 813 participants from the United Kingdom Biobank were used. The brain cortical features, including the cortical thickness (TH) and surface area (SA), were extracted from 51 665 patients across 60 cohorts. Surface area and TH were measured globally and in 34 functional regions using magnetic resonance imaging.

Methods: Bidirectional univariable MR (UVMR) was used to detect the causality between FD, VD, and brain cortex structure. Multivariable MR (MVMR) was used to adjust for confounding factors, including body mass index and blood pressure.

Main Outcome Measures: The global and regional measurements of brain cortical SA and TH.

Results: At the global level, higher VD is related to decreased TH ($\beta = -0.0140$ mm, 95% confidence interval: -0.0269 mm to -0.0011 mm, $P = 0.0339$). At the functional level, retinal FD is related to the TH of banks of the superior temporal sulcus and transverse temporal region without global weighted, as well as the SA of the posterior cingulate after adjustment. Vascular density is correlated with the SA of subregions of the frontal lobe and temporal lobe, in addition to the TH of the inferior temporal, entorhinal, and pars opercularis regions in both UVMR and MVMR. Bidirectional MR studies showed a causation between the SA of the parahippocampal and cauda middle frontal gyrus and retinal VD. No pleiotropy was detected.

Conclusions: Fractal dimension and VD causally influence the cortical structure and vice versa, indicating that the retinal microvasculature may serve as a biomarker for cortex structural changes. Our study provides insights into utilizing noninvasive fundus images to predict cortical structural deteriorations and neuropsychiatric disorders.

Financial Disclosure(s): The author(s) have no proprietary or commercial interest in any materials discussed in this article. *Ophthalmology Science 2024;4:100465*

Supplemental material available at www.ophthalmologyscience.org.

Cerebral disorders, such as Alzheimer's disease (AD), stroke, and Parkinson's disease (PD), have compromised human health and significantly diminished patients' quality of life, with corresponding alterations found in cortical thickness (TH) or surface area (SA) of certain cortex regions.[1–3] Early detection and prediction of cortex structure changes might provide early diagnosis of such diseases. The current examination, magnetic resonance imaging, is expensive and unable to predict future cortex structure changes; hence, an accessible and economical approach for diagnosing and predicting cerebral alternations is needed.

Given the anatomic and physiological similarities between the retinal microvasculature and that of others, fundus photographs allow noninvasive and economically valuable in vivo assessment of the microvasculature and are widely used in the diagnosis and prediction of hypertension,[4] diabetes,[5] and cardiovascular diseases.[6] Previous researches also revealed the interrelationship between the retina and brain by signifying their similar embryonic origins,[7] implying a promising perspective for understanding the origins and mechanisms of cerebral diseases while providing an insight into disease diagnosis and determination. Current imaging approaches have enabled the extraction of geometric and branching patterns of the retinal microvasculature, such as retinal fractal dimension (FD)[8–12] and vascular density (VD).[13,14] Such indices are associated with several neural disorders in previous cross-sectional analyses.[15–17] For example, early investigations found that decreased FD was significantly associated with cognitive dysfunction,[18] and lower spectrum FD in retinal microvasculature was correlated with a twofold risk of stroke.[19] More recent studies also showed that lower VD was found in patients

https://doi.org/10.1016/j.xops.2024.100465
ISSN 2666-9145/24

with moderate or severe cerebral small vessel disease compared with those with mild cerebral small vessel disease,[20] and that individuals with PD or AD exhibited reduced VD[21,22] in contrast to the normal population.

Although many observational studies suggested possible relationships between FD, VD, and cerebral alterations, the knowledge is sensitive to bias from confounding factors and reverse causation. The causation between retinal and neural pathology is still poorly understood. Mendelian randomization (MR) is a statistical approach for analyzing and estimating the relationships between risk factors and causal outcomes.[23] In MR analysis, genetic variants randomly allocated at conception are introduced as instrumental variables, providing a plausible method for investigating the causality assumptions between exposures and outcomes. As an extension of the MR method, 2-sample MR analysis employs summary statistics of genome-wide association studies (GWASs) instead of individual-level data, vastly improving the effectiveness of MR studies. Previous MR studies have revealed the causal relationships between albuminuria and the alteration of cortex structures,[24] as well as the link between educational attainment, structural brain reserve, and AD.[25] However, the influence of retinal vessel changes on cortex structure remains unclear.

Based on the publicly available GWAS data, we conducted a bidirectional MR analysis to detect the causality between FD, VD, and SA and TH of different cortex regions. Potential confounding factors were adjusted through multivariable MR (MVMR). Our results illustrate a comprehensive and accurate insight into the causal relationship between FD, VD, and SA and TH, and motivate the development of clinically applicable and explainable prediction and diagnosis of cortex structure changes on the basis of the features of retinal vessels in fundus photographs.

Methods

Study Design

A robust MR estimate is built on 3 MR assumptions: (1) the instrumental variables are strongly associated with exposure; (2) the instrumental variables are independent of confounders; and (3) the instrumental variables affect outcomes only through their effect on exposure and not through an alternative causal pathway. In this study, we designed a bidirectional univariable MR (UVMR) to identify the causal relationship and the direction of association between the retinal microvasculature and the brain cortical structure. Multivariable MR was also implemented to test the causation when adjusted by common confounding factors. A general overview of the MR design is presented in Figure 1.

Data Sources

The GWAS of retinal microvasculature was performed across 54 813 UK Biobank participants, recruited from 2006 to 2010 with existing genomic data, among which 50 223 (92%) self-reported as White, 1454 (2.7%) as Black, 1432 (2.6%) as South Asian, 213 (0.4%) as Chinese, and 1491 (2.7%) as other ethnicities. The original model adjusted age, age squared, sex, smoking status, and ancestry. A deep learning model was developed for vascular segmentation and feature extraction from the 97 895 fundus images across 54 813 participants. The branching complexity of retinal vasculature was measured with FD and VD (unit: standard deviation). Fractal dimension was calculated using a box-counting method[26] as previously proven applicable for the retina.[27] Vascular density was defined as the total number of pixels in the segmented vessels given a fixed dimension of 320 × 320 pixels for each image.[28] Genome-wide association study was then performed for FD and VD to generate genetic variant association estimates.[28]

The GWAS data of brain cortical structural indices were obtained from 51 665 individuals across 60 cohorts,[29] primarily of European descent (94%).

The brain cortical SA (unit: mm^2) and TH (unit: mm) were measured from whole-brain T1-weighted magnetic resonance imaging scans with the FreeSurfer magnetic resonance imaging-processing software, and harmonization between cohorts was conducted through detailed image processing and quality control protocols by the previous researchers. The 34 brain regions were defined based on the Desikan-Killiany atlas to establish standardized gyral-based neuroanatomical partitions of the cortex.[30] The regional measurements were averaged between both hemispheres.[31] Age, age squared, sex, sex-by-age and age squared interactions, ancestry, diagnostic status (when the original cohort was a case-control design), and dummy variables for scanner were adjusted in the original model. The heterogeneity assessment of the meta-analysis was presented in the original article. We performed MR analysis on TH and SA of the entire cortex and the 34 brain cortical regions. In addition to direct measurements of the regional SA and TH, global weighted estimates were obtained by including the global measure of SA or TH as an additional covariate in the GWAS analyses to indicate the SA and TH of specific regions across the SA and TH of the entire brain.

Selection of Genetic Instruments

Single nucleotide polymorphisms (SNPs) robustly associated with exposures were selected via the following criteria: (1) a GWAS-correlated P value threshold of 5×10^{-8}, and (2) a linkage disequilibrium r^2 of < 0.001 and < 1 MB from the index variant.

According to Zekavat et al,[28] 2 sets of genetic instruments indicating different aspects of retinal microvasculature were selected, including (1) 7 genome-wide−significant SNPs representing FD (Table S1, available at https://www.ophthalmologyscience.org) and (2) 13 genome-wide−significant SNPs representing VD (Table S2, available at https://www.ophthalmologyscience.org). Single nucleotide polymorphisms rs16891982, rs1711954, and rs16891982 in FD and SNPs rs62114548 in VD were removed for palindromic effect. In terms of cortical structure, we selected 369 genome-wide−significant SNPs (Table S3, available at https://www.ophthalmologyscience.org) according to Grasby's previous work.[29]

To avoid possible bias, we checked in PhenoScanner (www.phenoscanner.medschl.cam.ac.uk), a platform with comprehensive information on the association of genotype and phenotype, and removed SNPs associated with any of these potential confounders at genome-wide significance. For SNPs representing FD and VD, SNPs associated with neuropsychiatric diseases such as bipolar disorder and schizophrenia, education, drinking, and smoking were considered outcome-related and eliminated with a threshold of 5×10^{-8}. For SNPs representing cortical SA and TH, SNPs associated with ocular diseases such as diabetic retinopathy, glaucoma, and myopia were considered outcome-related and eliminated with a threshold of 5×10^{-8}. The MR Pleiotropy RESidual Sum and Outlier test was applied to remove the underlying horizontal pleiotropic outliers before each MR analysis.

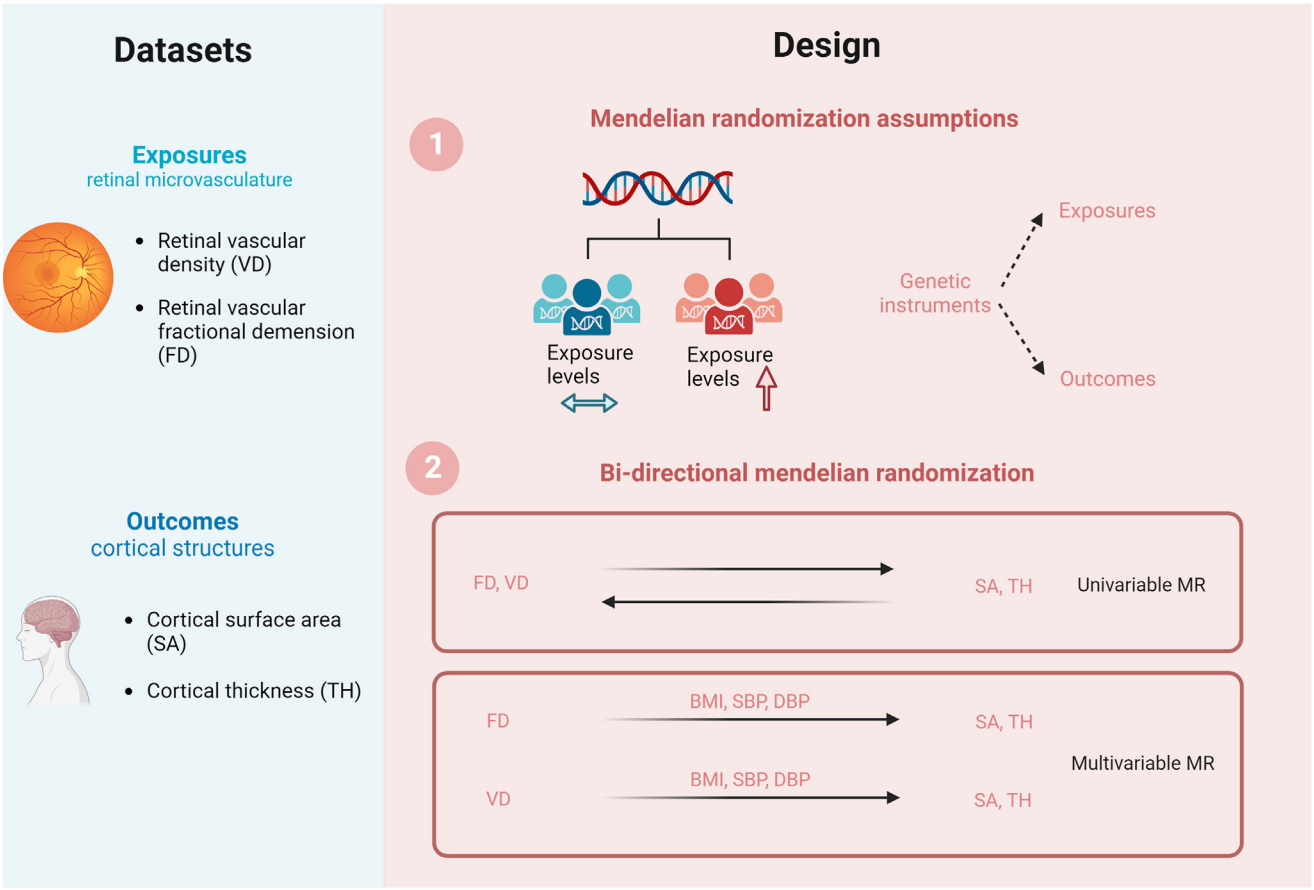

Figure 1. Study framework of the Mendelian randomization (MR) study. This study revealed the bidirectional causal relationship between retinal microvasculature and the brain cortical structure as defined using magnetic resonance imaging-measured brain cortical surface area and thickness. Created with BioRender.com. BMI = body mass index; DBP = diastolic blood pressure; SBP = systolic blood pressure.

MR Analyses

In the bidirectional UVMR analysis, the inverse-variance weighted method was used as the primary analytical strategy to investigate putative causal effects. To address variant heterogeneity and pleiotropic effects, we applied different two-sample MR approaches, including MR-Egger[32] and weighted median.[33] In the inverse-variance weighted analysis, the slope of the weighted regression of the SNP-outcome effects on the SNP-exposure effects, where the intercept was constrained to zero, represented the resulting estimate.

We further performed sensitivity analyses to ensure robust inferences. The MR-Egger intercept test and leave-one-out analysis were applied to assess horizontal pleiotropy for significant estimates. The Cochran's Q test was used to identify heterogeneity. A funnel plot was used to assess the potential directional pleiotropy.[32]

Multivariable MR was performed to identify the joint effect of other potential exposures on the causal relationship between the retina and the brain. Blood pressure was reported to have an adverse effect on cognitive function,[34] and the SNPs related to systolic blood pressure (SBP) and diastolic blood pressure (DBP) were obtained from the GWAS by Evangelou et al.[35] As previous studies reported a causal relationship between body mass index (BMI) and cortical structure;[36,37] BMI was also included in the MVMR using the GWAS data by Yengo et al.[38]

In cases of multiple comparisons, the *P* value is corrected with the Benjamini-Hochberg Procedure.[39] A raw *P* value < 0.05 is considered nominally significant, and a corrected *P* value < 0.05 is considered statistically significant. No missing data was involved in this study. All analyses were performed using the TwoSampleMR (version 0.4.25) and MR Pleiotropy RESidual Sum and Outlier (version 1.0) packages in R (version 3.6.1).

Availability of Data and Materials

The datasets analyzed during the current study are available in the following repositories: data regarding retinal parameters were obtained from the original research article [https://doi.org/10.1161/CIRCULATIONAHA.121.057709], and data regarding cortical structure were obtained from the ENIGMA Consortium [https://enigma.ini.usc.edu/research/download-enigma-gwas-results/]. This study exploits publicly available deidentified data from previous studies. The original researches were granted approvals from ethics committees with respect to human experimentation. No separate ethical approval was required in this study.

Results

A comprehensive MR analysis was performed to identify the causal relationship between the retina microvasculature and the brain structure. The characteristics of all selected SNPs were presented in Tables S1−S3 (available at https://

www.ophthalmologyscience.org). F-statistic values of all genetic instruments were > 10, effectively avoiding bias from weak instruments.[40]

Causal Effect of Retinal Microvasculature on Cerebral Cortex Structure

The results of UVMR analysis to explore the causal effect of retinal microvasculature on cerebral cortex structure were presented in Figures 2, 3, Figs S4−S19 and Tables 4, 5, Table S6 (available at https://www.ophthalmologyscience.org). At the global level, MR-PRESSO analysis identified SNP rs8070929 as an outlier for VD on TH. After removing rs8070929, we found that higher VD is nominally associated with decreased global TH (β = −0.0140 mm, 95% confidence interval [CI]: −0.0269 mm to −0.0011 mm, P = 0.0339). Conversely, no causal relationship was found between VD and global SA. Fractal dimension had no causal relationship with both global TH and SA.

At the functional region level, higher FD is nominally associated with increased SA of posterior cingulate gyrus (β = 18.8775 mm^2, 95% CI: 6.9460 mm^2−30.8089 mm^2, P = 0.0019) and decreased SA of superior parietal region (β = −61.6898 mm^2, 95% CI: −103.9914 mm^2 to −19.3883 mm^2, P = 0.0043). Surface area of the insula, pars orbitalis, postcentral, fusiform without global weighted, and rostral anterior cingulate regions were nominally influenced by FD. Fractal dimension was also found suggestively associated with TH of the transverse temporal without global weighted, pericalcarine without global weighted, and banks of the superior temporal sulcus regions without global weighted, along with the superior frontal gyrus as shown in Table 4 and Figure 2. On the other hand, it was statistically significant that higher VD is associated with decreased SA of the lateral orbitofrontal gyrus (β = −55.8853 mm, 95% CI: −86.7411 mm to −25.0296 mm, P = 0.0004, P-corrected = 0.02659). An increased VD was also found nominally correlated with increased SA of the insula (β = 33.1570 mm, 95% CI: 12.2046 mm−54.1093 mm, P = 0.0019), as well as decreased SA of various regions across the frontal, parietal, and temporal lobes. The results also suggested that VD was nominally associated with the TH of the posterior cingulate and the pars opercularis regions, along with multiple other gyri. Details of the various brain regions potentially influenced by VD are presented in Table 5 and Figure 3.

Causal Effect of Cerebral Cortex Structure on Retinal Microvasculature

The results of UVMR analysis to explore the causal effect of cerebral cortex structure on retinal microvasculature were presented in Table S7 and Figs S20−S28 (available at https://www.ophthalmologyscience.org). At the global level, no causal relationship was found between SA, TH and FD, and VD. At the functional region level, enlarged SA of the caudal middle frontal region with global weighted was nominally associated with decreased FD (β = −0.0005, 95% CI: −0.00097 to −0.00012, P = 0.0107). It was shown that increased TH of the middle temporal gyrus with global weighted potentially caused increased FD (β = 1.5623, 95% CI: 0.2294−2.8951, P = 0.0191), and increased SA of banks of the superior temporal sulcus with global weighted nominally leads to higher FD (β = 0.001524, 95% CI: 0.000002−0.0030, P = 0.0452).

As for the causation of cortical structure on VD, extended SA of the parahippocampal gyrus with global weighted significantly influenced VD (β = 0.0038, 95% CI: 0.0016−0.0061, P = 0.0006, P-corrected = 0.0151). Increased SA of the caudal middle frontal region with global weighted was also significantly correlated with decreased VD (β = −0.00071, 95% CI: −0.0011 to −0.0003, P = 0.0011, P-corrected = 0.0151). The SA of the superior temporal gyrus with global weighted has a nominal causation effect on retinal VD (β = −0.00045, 95% CI: −0.00078 to −0.00012, P = 0.0066), and the SA of the transverse temporal region with global weighted could potentially affect VD (β = −0.00264, 95% CI: −0.0049 to −0.0004, P = 0.0189). Increased TH of the middle temporal gyrus with global weighted was found nominally significant in increasing VD (β = 1.5894, 95% CI: 0.0485−3.1303, P = 0.0391).

MVMR Analysis

In order to eliminate the potential confounding effects, we conducted MVMR analysis to adjust for BMI, SBP, and DBP. The results of MVMR analysis were presented in Figures 2, 3, Figs S29−S37, Tables 8, 9, and Tables S10−S12 (available at https://www.ophthalmologyscience.org). After controlling for BMI, FD remains significantly correlated with TH of the pericalcarine (β = −0.0121, 95% CI: −0.0185 to −0.0058, P = 0.0001, P-corrected = 0.0012) and the transverse temporal region (β = −0.0471, 95% CI: −0.0794 to −0.0149, P = 0.0035, P-corrected = 0.0186), and nominally correlated with the banks of the superior temporal sulcus (β = −0.0018, 95% CI: −0.0031 to −0.0004, P = 0.0093), all without global weighted. Fractal dimension was also found significantly correlated with SA of posterior cingulate (β = 7.4092, 95% CI: 6.9067−7.9117, P < 0.001, P-corrected < 0.001). The causation from VD to SA of the caudal anterior cingulate (β = −9.7795, 95% CI: −15.6978 to −3.8612, P = 0.0010, P-corrected = 0.0081), rostral anterior cingulate (β = −19.2294, 95% CI: −31.3118 to −7.1470, P = 0.0015, P-corrected = 0.0101), and both SA and TH of caudal middle frontal region (SA: β = −67.3518, 95% CI: −112.6739 to −22.0296, P = 0.0030, P-corrected = 0.0170; TH: β = −0.0244, 95% CI: −0.0407 to −0.0081, P = 0.0028, P-corrected = 0.0002) without global weighted remains statistically significant after BMI was controlled. Other cortical regions presenting causational relationships were presented in Table S10 (available at https://www.ophthalmologyscience.org). Systolic blood pressure and DBP were adjusted respectively in the MVMR analysis. After correcting SBP, we found statistically significant causation of FD on SA of posterior cingulate gyrus (β = 13.3196, 95% CI: 5.7061−20.9330, P =

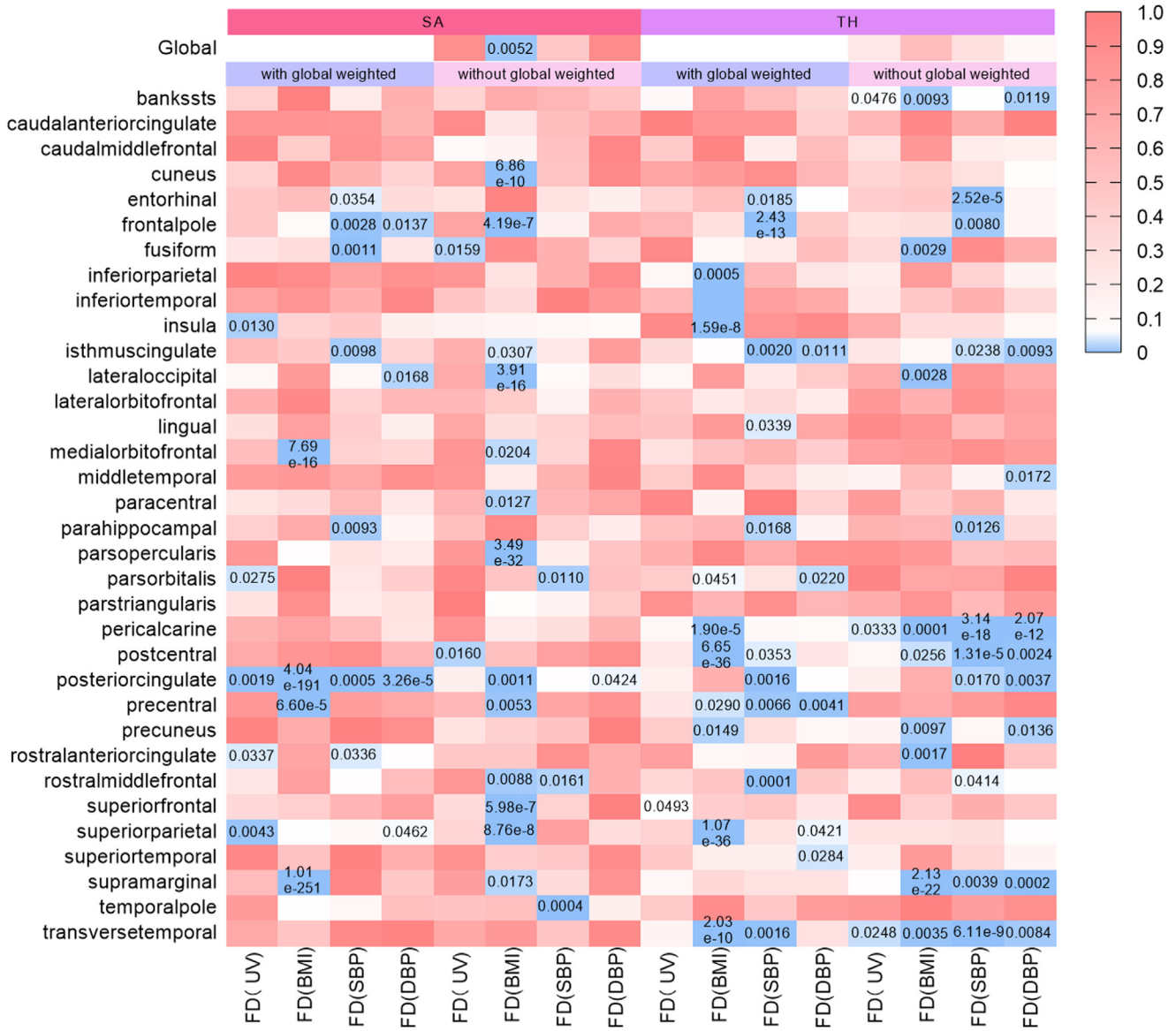

Figure 2. Mendelian randomization (MR) analysis results of retinal fractal dimension (FD). The inverse-variance weighted (IVW) estimates from retinal vascular FD on brain structure as defined using magnetic resonance imaging-measured brain cortical surface area (SA) and thickness (TH). Univariable MR IVW *P* values and multivariable MR IVW *P* values adjusted for body mass index (BMI), systolic blood pressure (SBP), and diastolic blood pressure (DBP) are shown in the heatmap. The color of each block represents the IVW-derived *P* values of every MR analysis, *P* value of < 0.05 were shown in blue and *P* values of > 0.05 were shown in red or white. *P* value < 0.05 is set as significant.

0.0005, *P*-corrected = 0.0161), TH of pericalcarine (β = 0.0118, 95% CI: −0.0145 to −0.0091, $P < 0.001$, *P*-corrected < 0.001), and transverse temporal region without global weighted (β = −0.0364 mm, 95% CI: −0.0489 to −0.0239, $P < 0.001$, *P*-corrected < 0.001). Nominal significant causation on SA of rostral anterior cingulate gyrus (β = −12.6810, 95% CI: −24.6143 to −0.7477, $P = 0.0336$) was presented. Regarding VD, statistically significant correlation with SA of the inferior parietal (β = −90.7199, 95% CI: −121.7587 to −59.6812, $P < 0.001$, *P*-corrected < 0.001) and the middle temporal regions (β = −49.6114, 95% CI: −74.5106 to −24.7121, $P = 0.0011$, *P*-corrected = 0.0371) without global weighted was found. Other nominal correlations were found between VD and the studied brain regions, as presented in Table S11 (available at https://www.ophthalmologyscience.org).

When adjusted for DBP, FD is significantly related with TH of pericalcarine (β = −0.0120, 95% CI: −0.0154 to −0.0086, $P < 0.001$, *P*-corrected < 0.001) and SA of posterior cingulate without global weighted. Fractal dimension is nominally correlated with TH of the transverse temporal region (β = 17.5683, 95% CI: 9.1114−26.0252, $P < 0.001$, *P*-corrected < 0.001) and the banks of the superior

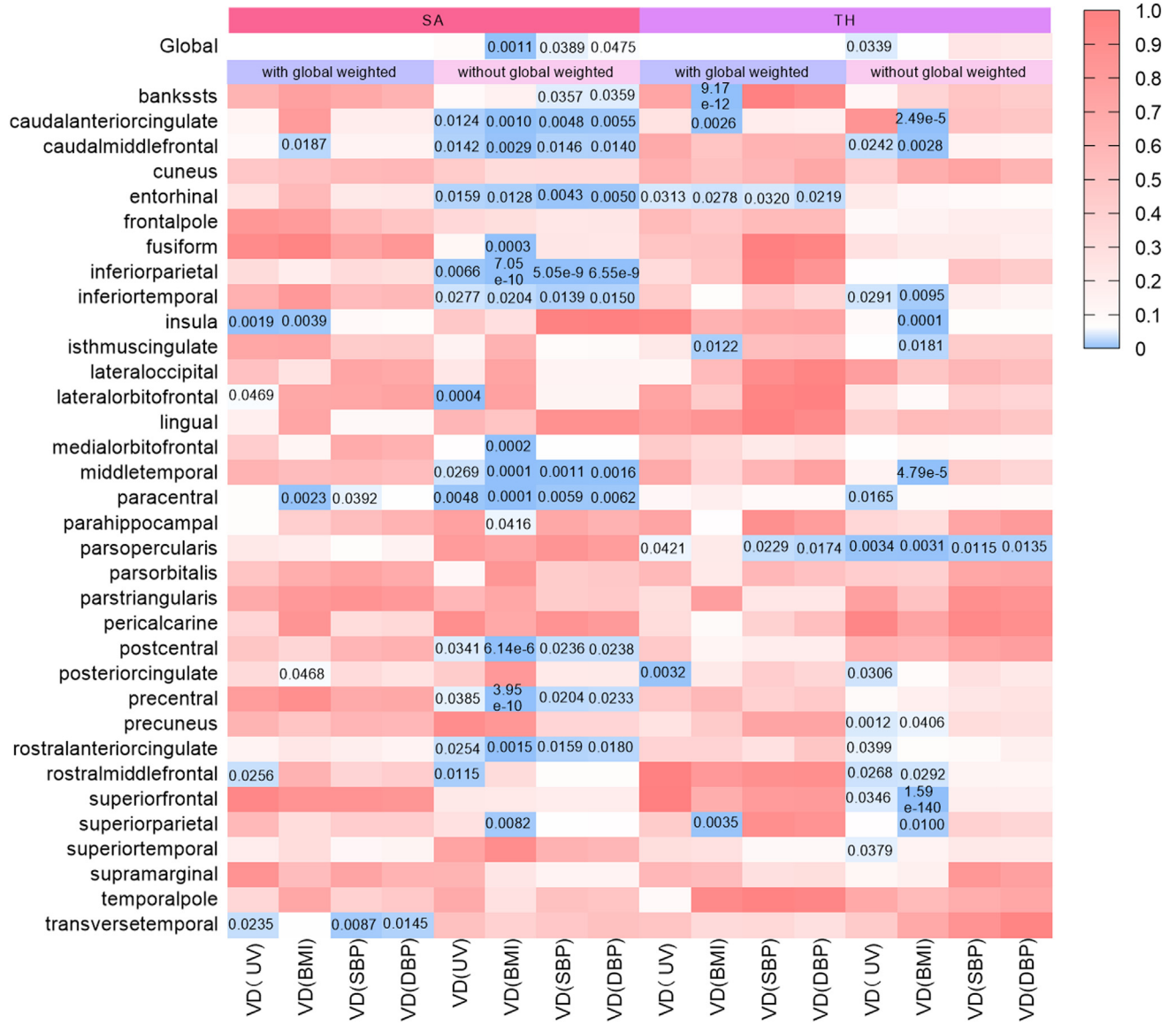

Figure 3. Mendelian randomization (MR) analysis results of retinal vessel density (VD). The inverse-variance weighted (IVW) estimates from retinal VD on brain structure as defined using magnetic resonance imaging-measured brain cortical surface area (SA) and thickness (TH). Univariable MR IVW *P* values and multivariable MR IVW *P* values adjusted for body mass index (BMI), systolic blood pressure (SBP), and diastolic blood pressure (DBP) are shown in the heatmap. The color of each block represents the IVW-derived *P* values of every MR analysis, *P* value of < 0.05 were shown in blue and *P* values of $>$ 0.05 were shown in red or white. *P* value < 0.05 is set as significant.

temporal sulcus ($\beta = -0.0130$, 95% CI: -0.0233 to -0.0027, $P = 0.0119$) without global weighted. Vascular density was found significantly associated with the SA of the inferior parietal region without global weighted ($\beta = -91.3525$, 95% CI: -202.5991 to -59.8629, $P < 0.001$, *P*-corrected < 0.001). There are nominally significant causations of VD on SA of the middle temporal, entorhinal, caudal anterior cingulate, paracentral, caudal middle frontal, inferior temporal, rostral anterior cingulate, precentral, and postcentral regions without global weighted, and SA of transverse temporal. The causal relationship between VD and TH of pars opercularis and entorhinal and pars opercularis without global weighted was also nominally significant. Details of the MVMR analysis adjusting for DBP are presented in Table S12 (available at https://www.ophthalmologyscience.org).

Sensitivity Analysis

For significant estimates, Cochran's Q test, MR-Egger intercept test, leave-one-out analyses, and funnel plot were used to assess horizontal pleiotropy. Regarding the potential causal relationship of retinal microvasculature to brain structure, all Cochran Q-derived *P* values were > 0.05,

Table 4. Significant Univariable MR Estimates From Retinal Vascular Fractal Dimension on Genetically Predicted Cortical Structure

Outcome	IVW-Derived *P* Value	β (95% Confidence Intervals)	Cochran's Q-Derived *P* Value	MR-Egger Intercept Derived *P* Value
TH of banks of the superior temporal sulcus w/o	0.0476	−0.0165 mm (−0.0329 mm to −0.0002 mm)	0.8756	0.7535
SA of fusiform w/o	0.0159	−105.1013 mm^2 (−190.5030 mm^2 to −19.6996 mm^2)	0.4626	N/A*
SA of insula	0.0130	29.3737 mm^2 (6.1888 mm^2–52.5587 mm^2)	0.1601	0.1836
SA of pars orbitalis	0.0275	23.5499 mm^2 (2.6147 mm^2–44.4851 mm^2)	0.2826	0.9126
TH of pericalcarine w/o	0.0333	−0.0129 mm (−0.0248 mm to −0.00108 mm)	0.714	0.4573
SA of postcentral w/o	0.0160	−128.9417 mm^2 (−233.8096 mm^2 to −24.0441 mm^2)	0.7484	N/A*
SA of posterior cingulate	0.0019	18.8775 mm^2 (6.9460 mm^2–30.8089 mm^2)	0.6377	0.5443
SA of rostral anterior cingulate	0.0337	−13.2703 mm^2 (−25.5192 mm^2 to −1.0213 mm^2)	0.218	0.4911
TH of superior frontal	0.0493	0.0096 mm (0.0047 mm–0.0145 mm)	0.9219	0.5767
SA of superior parietal	0.0043	−61.6898 mm^2 (−103.9914 mm^2 to −19.3883 mm^2)	0.7533	0.5647
TH of transverse temporal w/o	0.0248	−0.0247 mm (−0.0463 mm to −0.0031 mm)	0.7733	0.8603

IVW = inverse-variance weighted; MR = Mendelian randomization; SA = cortical surface area; TH = cortical thickness; w/o = without global weighted. All regions stated with w/o refer to the value without global weighted, and the rest indicates the value with global weighted. Nominal significant estimate is defined as IVW-derived $P < 0.05$.
*MR-Egger test is invalid for single nucleotide polymorphism numbers < 3.

showing no heterogeneity (Table S6, available at https://www.ophthalmologyscience.org). There was no evidence of heterogeneity in all other results where Cochran Q-derived *P* values were > 0.05. All *P* values of MR-Egger intercept tests were > 0.05, indicating no horizontal pleiotropy. The funnel plots were mostly symmetrical as shown in Figs S6 and S14–S16. Leave-one-out analyses showed no distortion, indicating that the estimates were not biased by any single SNP (Figs S7, S17–S19, available at https://www.ophthalmologyscience.org).

For the reverse correlation between cortical structure and the retina, similar approach was implemented for sensitivity analysis. Cochran's Q derived *P* values were all > 0.05, indicating no heterogeneity (Table S7, available at https://www.ophthalmologyscience.org). All *P* values of MR-Egger intercept tests were > 0.05, indicating no horizontal pleiotropy. The funnel plots showed no pleiotropy, and no distortion was found in the corresponding leave-one-out plots (Figs S22, S23, S26, S27, available at https://www.ophthalmologyscience.org).

Discussion

This study is the first large-scale bidirectional MR analysis that comprehensively determines the causal relationship between retinal microvasculature and brain cortical structure. The results show that retinal FD and VD could affect the brain cortex and vice versa, which endorsed the findings of earlier observational studies that indicated the pathophysiologic interactions between retinal microvasculature and brain structure. The causal relationship persists after accounting for BMI and blood pressure in the MVMR analysis. Consequently, our study establishes a clinically applicable and comprehensible theory for predicting cortex structures or future neuropsychiatric disorders on the basis of retinal vascular features in fundus photographs.

The rationale of this study is based on the widely accepted concept that retinal vascular health mirrors cerebral circulation. The brain and the retina, both part of the central nervous system (CNS), share many similarities in various aspects. The physiological functions of the CNS rely on communication among the complex network of constituent neurological cells. Vascularization of the CNS ensures adequate delivery of oxygen and nutrients to build up and maintain homeostasis of high energy-demanding neuronal networks. On the other hand, the blood-CNS interfaces, including the blood-brain barrier and blood-retinal barrier, create a defined microenvironment and establish the CNS as an immunologically privileged site.[41–44] Loss of blood-brain barrier or blood-retinal barrier integrity has been recognized in a wide variety of clinical contexts, including stroke,[45] neurodegenerative disorders,[46] diabetes,[47] and traumatic brain injury.[48] Due to developmental and functional commonalities between the blood-brain barrier and blood-retinal barrier[49] retinal vasculature abnormality has previously been identified in various neuropsychiatric disorders including AD,[50] PD,[51] bipolar disorder, autism spectrum disorders,[52,53] and schizophrenia.[54,55] The retina offers a unique window for observing neural and vascular structures in vivo. Considering the affordability and easy accessibility of retinal investigative procedures, fundus microvascular examinations could serve as a potential screening tool to identify individuals at risk for adverse cerebrovascular events.

Our result has further elucidated that retinal FD and VD causally influence various cerebral regions associated with neurocognitive deficits. Vascular density notably influenced the TH of the entorhinal cortex, a region exhibiting functional and histological alterations in preclinical AD.[56] Additionally, the SA of the caudal middle frontal region,[57] the SA of the

Table 5. Significant Univariable MR Estimates From Retinal Vascular Density on Genetically Predicted Cortical Structure

Outcome	IVW-Derived *P* Value	β (95% Confidence Intervals)	Cochran's Q-Derived *P* Value	MR-Egger Intercept Derived *P* Value
Global TH	0.0339	−0.0140 mm (−0.0269 mm to −0.0011 mm)	0.0932	0.7482
SA of caudal anterior cingulate w/o	0.0124	−15.9136 mm^2 (−28.3884 mm^2 to −3.4388 mm^2)	0.7711	0.9318
SA of caudal middle frontal w/o	0.0142	−58.4872 mm^2 (−105.2478 mm^2 to −11.7265 mm^2)	0.0617	0.7482
TH of caudal middle frontal w/o	0.0242	−0.0180 mm (−0.0338 mm to −0.0024 mm)	0.3469	0.1557
SA of entorhinal w/o	0.0159	−8.7867 mm^2 (−15.9318 mm^2 to −1.6416 mm^2)	0.568	0.6871
TH of entorhinal	0.0313	0.0355 mm (0.0032 mm−0.0678 mm)	0.7539	0.4465
SA of inferior parietal w/o	0.0066	−86.8278 mm^2 (−149.5124 mm^2 to −24.1433 mm^2)	0.9926	0.7939
SA of inferior temporal w/o	0.0277	−50.3086 mm^2 (−95.0874 mm^2 to −5.5297 mm^2)	0.3346	0.8055
TH of inferior temporal w/o	0.0291	−0.0188 mm (−0.0357 mm to −0.0019 mm)	0.3226	0.1557
SA of insula	0.0019	33.1570 mm^2 (12.2046 mm^2−54.1093 mm^2)	0.1972	0.1247
SA of lateral orbitofrontal	0.0469	−26.2679 mm^2 (−53.0355 mm^2 to −0.3603 mm^2)	0.0819	0.9073
SA of lateral orbitofrontal w/o	0.0004*	−55.8853 mm^2 (−86.7411 mm^2 to −25.0296 mm^2)	0.4565	0.3320
SA of middle temporal w/o	0.0269	−44.1638 mm^2 (−83.2919 mm^2 to −5.0358 mm^2)	0.8439	0.8222
SA of paracentral w/o	0.0048	−27.6552 mm^2 (−46.8721 mm^2 to −8.4383 mm^2)	0.4496	0.581
TH of paracentral w/o	0.0165	−0.0233 mm (−0.0425 mm to −0.0043 mm)	0.119	0.6916
TH of pars opercularis	0.0421	−0.0128 mm (−0.0251 mm to −0.0005 mm)	0.0820	0.6026
TH of pars opercularis w/o	0.0034	−0.0248 mm (−0.0415 mm to −0.0082 mm)	0.1621	0.1372
SA of postcentral w/o	0.0341	−68.7930 mm^2 (−132.4337 mm^2 to −5.1523 mm^2)	0.0378	0.2773
TH of posterior cingulate	0.0032	−0.0236 mm (−0.0393 mm to −0.0079 mm)	0.2678	0.2275
TH of posterior cingulate w/o	0.0281	−0.0212 mm (−0.0405 mm to −0.0019 mm)	0.0730	0.1994
SA of precentral w/o	0.0385	−64.0805 mm^2 (−124.7799 mm^2 to −3.3811 mm^2)	0.1469	0.3086
TH of precuneus w/o	0.0333	−0.0181 mm (−0.0349 mm to −0.0014 mm)	0.1130	0.8220
SA of rostral anterior cingulate w/o	0.0254	−16.3637 mm^2 (−30.7088 mm^2 to −2.0187 mm^2)	0.3245	0.8222
TH of rostral anterior cingulate w/o	0.0399	−0.0230 mm (−0.0449 mm to −0.0011 mm)	0.3192	0.6399
SA of rostral middle frontal	0.0256	−57.1654 mm^2 (−107.3640 mm^2 to −6.9667 mm^2)	0.2302	0.7792
SA of rostral middle frontal w/o	0.0115	−130.2193 mm^2 (−231.1787 mm^2 to −29.2598 mm^2)	0.0745	0.5491
TH of rostral middle frontal w/o	0.0268	−0.0147 mm (−0.0279 mm to −0.0017 mm)	0.4157	0.8016
TH of superior frontal w/o	0.0346	−0.0164 mm (−0.0316 mm to −0.0012 mm)	0.4169	0.8740
TH of superior temporal w/o	0.0379	−0.0179 mm (−0.0349 mm to −0.0010 mm)	0.3512	0.8199
SA of transverse temporal	0.0235	7.1631 mm^2 (0.9647 mm^2−13.3615 mm^2)	0.1597	0.8055

IVW = inverse-variance weighted; MR = Mendelian randomization; SA = cortical surface area; TH = cortical thickness; w/o = without global weighted. All regions stated with w/o refer to the value without global weighted, and the rest indicates the value with global weighted. Nominal significant estimate is defined as IVW-derived $P < 0.05$.
*Statistically significant with *P*-corrected < 0.05 using the Benjamini-Hochberg Procedure.

inferior parietal region,[58] and the TH of the banks of the superior temporal sulcus,[59] which present morphology changes in AD, were also causally impacted by retinal vessel alternations after adjustments. The cingulate gyrus participates in emotion and memory and was affected early in the onset of AD.[60,61] It was shown that the SA of the caudal anterior cingulate, rostral anterior cingulate, and posterior cingulate were all causally related to retinal microvasculature[62,63] even after correction of BMI, SBP, and DBP.

Table 8. Significant Multivariable Mendelian Randomization Estimates From Retinal Vascular Fractal Dimension on Genetically Predicted Cortical Structure

Outcome	*P* Value Adjusted for BMI	β (95% Confidence Intervals) Adjusted for BMI	*P* Value Adjusted for SBP	β (95% Confidence Intervals) Adjusted for SBP	*P* Value Adjusted for DBP	β (95% Confidence Intervals) Adjusted for DBP
TH of banks of the superior temporal sulcus w/o	0.0093*	−0.0018 mm (−0.0031 mm to −0.0004 mm)	0.0509	−0.0124 mm (−0.0252 mm to 0.0003 mm)	0.0119	−0.0130 mm (−0.0233 mm to −0.0027 mm)
SA of fusiform w/o	0.8992	5.542 mm^2 (−82.0159 mm^2 to 93.0995 mm^2)	0.6329	−12.9197 mm^2 (−61.0177 mm^2 to 41.1783 mm^2)	0.3714	−22.0730 mm^2 (−71.4634 mm^2 to 27.3174 mm^2)
SA of insula	0.3774	−17.4867 mm^2 (−57.1036 mm^2 to 22.1303 mm^2)	0.4486	14.8770 mm^2 (−24.3922 mm^2 to 54.1463 mm^2)	0.1699	23.8961 mm^2 (−10.9213 mm^2 to 58.7135 mm^2)
SA of pars orbitalis	0.0621	9.3081 mm^2 (−0.6691 mm^2 to 19.2854 mm^2)	0.2234	6.8475 mm^2 (−4.4010 mm^2 to 18.0960 mm^2)	0.4172	4.5048 mm^2 (−6.6001 mm^2 to 15.6097 mm^2)
TH of pericalcarine w/o	0.0001*	−0.0121 mm (−0.0185 mm to −0.0058 mm)	3.13 E-18*	−0.0118 mm (−0.0145 mm to −0.0091 mm)	2.06 E-12*	−0.0120 mm (−0.0154 mm to −0.0086 mm)
SA of postcentral w/o	0.5167	59.0112 mm^2 (−123.0002 mm^2 to 241.0225 mm^2)	0.7523	13.0306 mm^2 (−69.5481 mm^2 to 95.6092 mm^2)	0.8945	−4.5374 mm^2 (−72.9848 mm^2 to 63.9100 mm^2)
SA of posterior cingulate	4.04 E-191*	7.4092 mm^2 (6.9067 mm^2−7.9117 mm^2)	0.0005*	13.3196 mm (5.7061 mm−20.9330 mm)	3.26 E-05*	17.5683 mm^2 (9.1114 mm^2−26.0252 mm^2)
SA of rostral anterior cingulate	0.7209	−5.1177 mm^2 (−33.7673 mm^2 to 23.5319 mm^2)	0.0336	−12.6810 mm^2 (−24.6143 mm^2 to −0.7477 mm^2)	0.0636	−10.1661 mm^2 (−21.1250 mm^2 to 0.7928 mm^2)
TH of superior frontal	0.4218	−0.0043 mm (−0.0151 mm to 0.0064 mm)	0.4667	0.0038 mm (−0.0066 mm to 0.0141 mm)	0.2444	0.0048 mm (−0.0034 mm to 0.0129 mm)
SA of superior parietal	0.0542	−16.5866 mm^2 (−33.8154 mm^2 to 0.64222 mm^2)	0.1006	−44.7304 mm^2 (−99.2221 mm^2 to 9.7613 mm^2)	0.0462	−46.5347 mm^2 (−93.2253 mm^2 to 0.1558 mm^2)
TH of transverse temporal w/o	0.0035*	−0.0471 mm (−0.0794 mm to −0.0149 mm)	6.11 E-09*	−0.0364 mm (−0.0489 mm to −0.0239 mm)	0.0084	−0.0264 mm (−0.0465 mm to −0.0064 mm)

BMI = body mass index; DBP = diastolic blood pressure; SA = cortical surface area; SBP = systolic blood pressure; TH = cortical thickness; w/o = without global weighted.
All regions stated with w/o refer to the value without global weighted, and the rest indicates the value with global weighted. Nominal significant estimate is defined as inverse-variance weighted-derived $P < 0.05$.
*Statistically significant with *P*-corrected < 0.05 using the Benjamini-Hochberg Procedure.

Table 9. Significant Multivariable Mendelian Randomization Estimates From Retinal Vascular Density on Genetically Predicted Cortical Structure

Outcome	P Value Adjusted for BMI	β (95% Confidence Intervals) Adjusted for BMI	P Value Adjusted for SBP	β (95% Confidence Intervals) Adjusted for SBP	P Value Adjusted for DBP	β (95% Confidence Intervals) Adjusted for DBP
Global TH	0.0512	−0.0174 mm (−0.0352 mm to 0.0004 mm)	0.2443	−0.0095 mm (−0.0258 mm to 0.0068 mm)	0.2189	−0.0099 mm (−0.0261 mm to 0.0062 mm)
SA of caudal anterior cingulate w/o	0.0010*	−9.7795 mm^2 (−15.6978 mm^2 to −3.8612 mm^2)	0.0048	−14.2924 mm^2 (−24.4304 mm^2 to −4.1544 mm^2)	0.0054	−14.4764 mm^2 (−24.904 mm^2 to −4.0488 mm^2)
SA of caudal middle frontal w/o	0.0030*	−67.3518 mm^2 (−112.6739 mm^2 to −22.0296 mm^2)	0.0146	−56.4053 mm^2 (−102.6165 mm^2 to −10.194 mm^2)	0.0140	−56.6917 mm^2 (−102.8212 mm^2 to −10.5621 mm^2)
TH of caudal middle frontal w/o	0.0028*	−0.0244 mm (−0.0407 mm to −0.0081 mm)	0.1354	−0.0135 mm (−0.0316 mm to 0.0046 mm)	0.1237	−0.0139 mm (−0.0319 mm to 0.0041 mm)
SA of entorhinal w/o	0.0128	−8.3163 mm^2 (−15.0007 mm^2 to −1.6319 mm^2)	0.0043	−9.3245 mm^2 (−15.8635 mm^2 to −2.7856 mm^2)	0.0050	−9.3201 mm^2 (−15.9559 mm^2 to −2.6843 mm^2)
TH of entorhinal	0.0277*	0.046 mm (0.0042 mm−.0878 mm)	0.0320	0.0299 mm (0.002 mm−0.0578 mm)	0.0219	0.0312 mm (0.004 mm−0.0584 mm)
SA of inferior parietal w/o	7.05 E-10*	−90.0103 mm^2 (−119.2112 mm^2 to −60.8095 mm^2)	5.05 E-09*	−90.7199 mm^2 (−121.7587 mm^2 to −59.6812 mm^2)	6.55 E-09*	−91.3525 mm^2 (−202.5991 mm^2 to −59.8629 mm^2)
SA of inferior temporal w/o	0.0204	−49.6679 mm^2 (−92.4888 mm^2 to −6.8469 mm^2)	0.0130	−54.8646 mm^2 (−99.4909 mm^2 to −10.2382 mm^2)	0.0150	−54.7616 mm^2 (−99.8101 mm^2 to −9.713 mm^2)
TH of inferior temporal w/o	0.0095*	−0.0267 mm (−0.0472 mm to −0.0061 mm)	0.1757	−0.0136 mm (−0.0337 mm to 0.0065 mm)	0.1262	−0.0146 mm (−0.0336 mm to 0.0045 mm)
SA of insula	0.0039*	44.2738 mm^2 (13.5521 mm^2−74.9955 mm^2)	0.0884	22.6122 mm^2 (−3.9312 mm^2 to 49.1557 mm^2)	0.0797	23.0367 mm^2 (−3.2580 mm^2 to 49.3313 mm^2)
SA of lateral orbitofrontal	0.7002	12.5721 mm^2 (−52.7318 mm^2 to 77.8761 mm^2)	0.7050	−7.1629 mm^2 (−44.9998 mm^2 to 30.6740 mm^2)	0.7445	−6.2020 mm^2 (−44.2633 mm^2 to 31.8592 mm^2)
SA of lateral orbitofrontal w/o	0.7495	−13.2612 mm^2 (−96.3450 mm^2 to 69.8217 mm^2)	0.1256	−35.0057 mm^2 (−80.7091 mm^2 to 10.6977 mm^2)	0.1290	−34.3993 mm^2 (−79.7236 mm^2 to 10.9250 mm^2)
SA of middle temporal w/o	6.75 E-05*	−49.6114 mm^2 (−74.5106 mm^2 to −24.7121 mm^2)	0.0011*	−48.8488 mm^2 (−78.7226 mm^2 to −18.975 mm^2)	0.0016	−49.5277 mm^2 (−80.861 mm^2 to −18.1943 mm^2)
SA of paracentral w/o	5.65 E-05*	−31.7137 mm^2 (−47.465 mm^2 to −15.9624 mm^2)	0.0059	−26.2377 mm^2 (−45.3061 mm^2 to −7.1693 mm^2)	0.0062	−26.0885 mm^2 (−45.1402 mm^2 to −7.0367 mm^2)
TH of paracentral w/o	0.0855	−0.0268 mm (−0.058 mm to 0.0044 mm)	0.0909	−0.0185 mm (−0.0404 mm to 0.0034 mm)	0.0868	−0.0186 mm (−0.0403 mm to 0.0031 mm)
TH of pars opercularis	0.2027	−0.0126 mm (−0.00324 mm to 0.0072 mm)	0.0229	−0.0136 mm (−0.0256 mm to −0.0017 mm)	0.0174	−0.0131 mm (−0.0241 mm to −0.0021 mm)
TH of pars opercularis w/o	0.0031*	−0.0272 mm (−0.0455 mm to −0.0088 mm)	0.0115	−0.022 mm (−0.0395 mm to −0.0046 mm)	0.0134	−0.0215 mm (−0.0388 mm to −0.0041 mm)
SA of postcentral w/o	6.14 E-06*	−86.0502 mm^2 (−124.1123 mm^2 to −47.988 mm^2)	0.0236	−70.9178 mm^2 (−133.5722 mm^2 to −8.2633 mm^2)	0.0238	−71.0137 mm^2 (−133.848 mm^2 to −8.1794 mm^2)
TH of posterior cingulate	0.2032	−0.0165 mm (−0.0424 mm to 0.0094 mm)	0.4199	−0.0079 mm^2 (−0.0273 mm^2 to 0.0116 mm^2)	0.3506	−0.0086 mm (−0.0270 mm to 0.0098 mm)
TH of posterior cingulate w/o	0.0763	−0.0271 mm (−0.0577 mm to −0.0035 mm)	0.2757	−0.0135 mm (−0.0384 mm to 0.0113 mm)	0.2203	−0.0146 mm (−0.0382 mm to 0.0092 mm)
SA of precentral w/o	3.95 E-10*	−56.8742 mm^2 (−75.056 mm^2 to −38.6924 mm^2)	0.0204	−68.2423 mm^2 (−127.0783 mm^2 to −9.4063 mm^2)	0.0233	−68.9826 mm^2 (−129.7926 mm^2 to −8.1725 mm^2)
TH of precuneus w/o	0.0406	−0.0185 mm (−0.0365 mm to −0.0004 mm)	0.3003	−0.0117 mm (−0.0342 mm to 0.0109 mm)	0.2781	−0.0121 mm (−0.0343 mm to 0.0102 mm)
SA of rostral anterior cingulate w/o	0.0015*	−19.2294 mm^2 (−31.3118 mm^2 to −7.147 mm^2)	0.0158	−15.8142 mm^2 (−28.9306 mm^2 to −2.6977 mm^2)	0.0180	−16.4330 mm^2 (−30.3312 mm^2 to −2.5348 mm^2)

Table 9. (Continued.)

Outcome	*P* Value Adjusted for BMI	β (95% Confidence Intervals) Adjusted for BMI	*P* Value Adjusted for SBP	β (95% Confidence Intervals) Adjusted for SBP	*P* Value Adjusted for DBP	β (95% Confidence Intervals) Adjusted for DBP
TH of rostral anterior cingulate w/o	0.0658	−0.0253 mm (−0.0528 mm to 0.0022 mm)	0.0862	−0.0183 mm (−0.0395 mm to 0.003 mm)	0.1589	−0.0172 mm (−0.0417 mm to 0.0072 mm)
SA of rostral middle frontal	0.8186	−0.0019 mm^2 (−0.0180 mm^2 to −0.0143 mm^2)	0.3683	−27.1315 mm^2 (−87.4426 mm^2 to 33.1797 mm^2)	0.4221	−24.6767 mm^2 (−85.1524 mm^2 to −36.7989 mm^2)
SA of rostral middle frontal w/o	0.3066	−81.6806 mm^2 (−241.4479 mm^2 to −78.1167 mm^2)	0.0706	−97.7230 mm^2 (−205.8390 mm^2 to 10.3929 mm^2)	0.0719	−95.9574 mm^2 (−122.8422 mm^2 to 10.6843 mm^2)
TH of rostral middle frontal w/o	0.0292*	−0.0194 mm (−0.0372 mm to −0.0016 mm)	0.1258	−0.0114 mm (−0.0262 mm to 0.0035 mm)	0.1190	−0.0116 mm (−0.0264 mm to 0.0033 mm)
TH of superior frontal w/o	1.59 E-140*	−0.0202 mm (−0.0217 mm to −0.0186 mm)	0.1719	−0.012 mm (−0.0296 mm to 0.0056 mm)	0.1661	−0.0121 mm (−0.0297 mm to 0.0054 mm)
TH of superior temporal w/o	0.1341	−0.0211 mm (−0.0493 mm to 0.0071 mm)	0.2170	−0.0128 mm (−0.0335 mm to 0.0079 mm)	0.2092	−0.0129 mm (−0.0335 mm to 0.0077 mm)
SA of transverse temporal	0.0506	8.2383 mm^2 (−0.1909 mm^2 to 16.6676 mm^2)	0.0087	7.6408 mm^2 (1.816 mm^2–13.4657 mm^2)	0.0144	7.3869 mm^2 (1.3453 mm^2–13.4286 mm^2)

BMI = body mass index; DBP = diastolic blood pressure; SA = cortical surface area; SBP = systolic blood pressure; TH = cortical thickness; w/o = without global weighted.
All regions stated with w/o refer to the value without global weighted, and the rest indicates the value with global weighted. Nominal significant estimate is defined as inverse-variance weighted-derived $P <$ 0.05.
*Statistically significant with P-corrected < 0.05 using the Benjamini-Hochberg Procedure.

Furthermore, structural alternations in the cingulate cortex were previously discovered in schizophrenia[64–66] and autism spectrum disorders. The impact of VD on the SA and TH of the inferior temporal gyrus, as well as the SA of the middle temporal gyrus and paracentral region, provides additional evidence for the correlation between retina and schizophrenia. The pars opercularis, a region related to autism spectrum disorders,[67] was also found to be impacted by VD after adjusting for confounding factors. Our analysis also confirmed the correlation between retinal indices and PD. Retinal VD was found to be associated with the SA of the precentral and paracentral gyri, regions affected in Lewy bodies and PD-associated dementia.[68]

In the bidirectional MR analysis framework, our results also underscored the mutual correlation between the eye and the brain. Specifically, the SA of 2 cerebral regions implicated in AD, the parahippocampal[69] and caudal middle frontal regions, was revealed to significantly influence the retinal vasculature. Prior research has consistently observed a concomitance of AD with retinal vascular anomalies, including changes in caliber and altered tortuosity.[70] However, the direct causal link between these organ-specific pathologies has not been established. This study is the first to explore the causality between ocular and cerebral pathophysiology using MR. It would be valuable for future studies to investigate the capacity of retinal microvasculature as a biomarker of neuropsychiatric disorders.

The connection between retinal vessel integrity and specific brain functions was also revealed in this study. We found that retinal FD is associated with TH alternation of the pericalcarine gyrus, which is consistent with previous findings that detected pericalcarine structural changes in blindsight subjects.[71] The inferior temporal cortex, crucial for visual perception including object identification and face recognition,[72] was shown to be causally affected by VD. Our findings indicated that retinal microvasculature deterioration may result in impairments extending beyond basic visual deficits to more sophisticated aspects of visual interpretation. In addition, we discovered that retinal VD and FD are associated with the morphological alternation of the transverse temporal gyrus, also known as the Heschl gyrus, which contains the primary auditory cortex.[73,74] We observed that a decrease in FD leads to augmented TH, hinting at potential compensatory adaptations in the primary auditory cortex in response to visual impairment. These findings enhance our understanding of the correlation between retinal vascular condition and sensory functions, providing a theoretical basis for future studies.

Notably, certain estimates varied from expectations. Low retinal FD and VD are traditionally considered significantly associated with higher risks for incident mortality, hypertension, congestive heart failure, renal failure, type 2 diabetes, sleep apnea, anemia, and multiple ocular conditions, namely myopia and retinal detachment.[28] In observational studies, high retinal FD and VD were significantly associated with better cognitive function and hence should lead to a larger TH.[17,19,22] However, this study demonstrated that genetically predicted higher VD leads to smaller global TH, and no significant association was detected with FD. Since VD was defined as the total number of pixels in the segmented

vessels given a fixed dimension of 320 × 320 pixels for each image, it mainly represents vessel diameter as opposed to branching complexity. Retinal venular dilatation is a clinical sign of diabetic retinopathy and retinal venous occlusion, and is associated with endothelial dysfunction, inflammation, and microvascular hypoxia.[5,75–77] We propose that the widening of venular caliber is the prominent contributor to cortical structure deterioration, explaining our result that higher VD is associated with smaller TH. Genome-wide association study analysis and further MR studies of other retinal microvasculature indices, such as the arterioles to venules ratio, could expand the understanding of how retinal vascular health influences cerebral function and structure.

There are several limitations to consider in this study. First, the enrolled patients were mostly European; hence, the causal relationship between retinal microvasculature and the brain cortical structure in other ethnic populations remains unknown. Second, the data from the United Kingdom Biobank leads to an estimated 19.52% overlap between the exposure and outcome studies, which may cause underlying bias. Third, although our findings report the causal relationship between retinal microvasculature and the brain cortical structure, the underlying mechanisms warrant further investigation. As the effect size was relatively small in the correlation analyzes between the retinal and cortical TH, future researchers should take caution in interpreting the results to avoid overestimation and consequent exaggeration of the correlation.

In conclusion, our investigation substantiates a bidirectional causal association between retinal FD and vessel density with regionally specific TH and SA, even after adjustment for confounders. These findings reinforce the prospective utility of retinal vasculature as a surrogate marker for neuropathological states, proposing that affordable and noninvasive fundus imaging could serve as a viable screening tool for neuropsychological diseases. This study could provide immediate value for clinical research and afford a robust foundation for the innovation of predictive methods and risk assessment tools for neuropsychiatric disorders.

Footnotes and Disclosures

Originally received: August 31, 2023.
Final revision: January 5, 2024.
Accepted: January 8, 2024.
Available online: January 24, 2024. Manuscript no. XOPS-D-23-00214.

[1] State Key Laboratory of Ophthalmology, Guangdong Provincial Key Laboratory of Ophthalmology and Vision Science, Guangdong Provincial Clinical Research Center for Ocular Diseases, Zhongshan Ophthalmic Center, Sun Yat-sen University, Guangzhou, Guangdong, China.

[2] Center for Precision Medicine, Sun Yat-sen University, Guangzhou, Guangdong, China.

[3] Zhongshan School of Medicine, Sun Yat-Sen University, Guangzhou, Guangdong, China.

[4] Hainan Eye Hospital and Key Laboratory of Ophthalmology, Zhongshan Ophthalmic Center, Sun Yat-sen University, Haikou, Hainan, China.

*X.W. and W.C.I. contributed equally in this study.

Disclosures:

All authors have completed and submitted the ICMJE disclosures form.

The authors have no proprietary or commercial interest in any materials discussed in this article.

This study was funded by the Science and Technology Planning Projects of Guangdong Province (No. 2021B1111610006), the National Natural Science Foundation of China (No. 82171035), the High-level Science and Technology Journals Projects of Guangdong Province (No. 2021B1212010003) and Science and Technology Program of Guangzhou (No. 202201020337). The funding organizations had no role in the following aspects: design and conduct of the study; the collection, management, analysis, and interpretation of the data; preparation, review, or approval of the manuscript; and decision to submit the manuscript for publication.

HUMAN SUBJECTS: No human subjects were included in this study. The original researches were granted approvals from ethics committees with respect to human experimentation. No separate ethical approval was required in this study. All data used in this Mendelian Randomization study is publicly available.

Author Contributions:

Conception and design: Wei, Iao, Haotian Lin

Data collection: Wei, Zhang, Zijie Lin

Analysis and interpretation: Wei, Iao, Zhang, Zijie Lin

Obtained funding: N/A

Overall responsibility: Wei, Iao, Haotian Lin

Abbreviations and Acronyms:
AD = Alzheimer's disease; **BMI** = body mass index; **CI** = confidence interval; **CNS** = central nervous system; **DBP** = diastolic blood pressure; **FD** = fractal dimension; **GWAS** = genome-wide association study; **MR** = Mendelian randomization; **MVMR** = multivariable Mendelian randomization; **PD** = Parkinson's disease; **SA** = surface area; **SBP** = systolic blood pressure; **SNP** = single nucleotide polymorphism; **TH** = cortical thickness; **UVMR** = univariable Mendelian randomization; **VD** = vascular density.

Keywords:
Cortical surface area, Cortical thickness, Fractal dimension, Vascular density.

Correspondence:
Haotian Lin, PhD, Zhongshan Ophthalmic Center, Sun Yat-sen University, Xian Lie South Road 54#, Guangzhou 510060, China. E-mail: linht5@mail.sysu.edu.cn.

References

1. Ballard C, Gauthier S, Corbett A, et al. Alzheimer's disease. *Lancet*. 2011;377:1019–1031.

2. Wang W, Jiang B, Sun H, et al. Prevalence, incidence, and mortality of stroke in China: results from a nationwide

population-based survey of 480 687 adults. *Circulation*. 2017;135:759−771.
3. Ascherio A, Schwarzschild MA. The epidemiology of Parkinson's disease: risk factors and prevention. *Lancet Neurol*. 2016;15:1257−1272.
4. Cheung CY, Ikram MK, Sabanayagam C, Wong TY. Retinal microvasculature as a model to study the manifestations of hypertension. *Hypertension*. 2012;60:1094−1103.
5. Cheung CY, Ikram MK, Klein R, Wong TY. The clinical implications of recent studies on the structure and function of the retinal microvasculature in diabetes. *Diabetologia*. 2015;58:871−885.
6. Cheung CY, Xu D, Cheng CY, et al. A deep-learning system for the assessment of cardiovascular disease risk via the measurement of retinal-vessel calibre. *Nat Biomed Eng*. 2021;5:498−508.
7. Jacobson M, Hirose G. Origin of the retina from both sides of the embryonic brain: a contribution to the problem of crossing at the optic chiasma. *Science*. 1978;202:637−639.
8. Avakian A, Kalina RE, Sage EH, et al. Fractal analysis of region-based vascular change in the normal and non-proliferative diabetic retina. *Curr Eye Res*. 2002;24:274−280.
9. Gardiner TA, Archer DB, Curtis TM, Stitt AW. Arteriolar involvement in the microvascular lesions of diabetic retinopathy: implications for pathogenesis. *Microcirculation*. 2007;14:25−38.
10. Grauslund J, Green A, Kawasaki R, et al. Retinal vascular fractals and microvascular and macrovascular complications in type 1 diabetes. *Ophthalmology*. 2010;117:1400−1405.
11. Liew G, Wang JJ, Cheung N, et al. The retinal vasculature as a fractal: methodology, reliability, and relationship to blood pressure. *Ophthalmology*. 2008;115:1951−1956.
12. Liew G, Gopinath B, White AJ, et al. Retinal vasculature fractal and stroke mortality. *Stroke*. 2021;52:1276−1282.
13. Alan G, Guenancia C, Arnould L, et al. Retinal vascular density as a novel biomarker of acute renal injury after acute coronary syndrome. *Sci Rep*. 2019;9:8060.
14. Hannappe MA, Arnould L, Méloux A, et al. Vascular density with optical coherence tomography angiography and systemic biomarkers in low and high cardiovascular risk patients. *Sci Rep*. 2020;10:16718.
15. Cheung CY, Tay WT, Ikram MK, et al. Retinal microvascular changes and risk of stroke: the Singapore Malay Eye Study. *Stroke*. 2013;44:2402−2408.
16. Ong YT, De Silva DA, Cheung CY, et al. Microvascular structure and network in the retina of patients with ischemic stroke. *Stroke*. 2013;44:2121−2127.
17. Doubal FN, MacGillivray TJ, Patton N, et al. Fractal analysis of retinal vessels suggests that a distinct vasculopathy causes lacunar stroke. *Neurology*. 2010;74:1102−1107.
18. Cheung CY, Ong S, Ikram MK, et al. Retinal vascular fractal dimension is associated with cognitive dysfunction. *J Stroke Cerebrovasc Dis*. 2014;23:43−50.
19. Kawasaki R, Che Azemin MZ, Kumar DK, et al. Fractal dimension of the retinal vasculature and risk of stroke: a nested case-control study. *Neurology*. 2011;76:1766−1767.
20. Ma L, Wang M, Chen H, et al. Association between retinal vessel density and neuroimaging features and cognitive impairment in cerebral small vessel disease. *Clin Neurol Neurosurg*. 2022;221:107407.
21. Robbins CB, Thompson AC, Bhullar PK, et al. Characterization of retinal microvascular and choroidal structural changes in Parkinson disease. *JAMA Ophthalmol*. 2021;139:182−188.
22. Yan Y, Wu X, Wang X, et al. The retinal vessel density can reflect cognitive function in patients with Alzheimer's disease: evidence from optical coherence tomography angiography. *J Alzheimers Dis*. 2021;79:1307−1316.
23. Smith GD, Ebrahim S. 'Mendelian randomization': can genetic epidemiology contribute to understanding environmental determinants of disease? *Int J Epidemiol*. 2003;32:1−22.
24. Chen X, Kong J, Pan J, et al. Kidney damage causally affects the brain cortical structure: a Mendelian randomization study. *EBioMedicine*. 2021;72:103592.
25. Seyedsalehi A, Warrier V, Bethlehem RAI, et al. Educational attainment, structural brain reserve and Alzheimer's disease: a Mendelian randomization analysis. *Brain*. 2023;146:2059−2074.
26. Meyer HV, Dawes TJW, Serrani M, et al. Genetic and functional insights into the fractal structure of the heart. *Nature*. 2020;584:589−594.
27. Huang F, Dashtbozorg B, Zhang J, et al. Reliability of using retinal vascular fractal dimension as a biomarker in the diabetic retinopathy detection. *J Ophthalmol*. 2016;2016:6259047.
28. Zekavat SM, Raghu VK, Trinder M, et al. Deep learning of the retina enables phenome- and genome-wide analyses of the microvasculature. *Circulation*. 2022;145:134−150.
29. Grasby KL, Jahanshad N, Painter JN, et al. The genetic architecture of the human cerebral cortex. *Science*. 2020;367:eaay6690.
30. Desikan RS, Ségonne F, Fischl B, et al. An automated labeling system for subdividing the human cerebral cortex on MRI scans into gyral based regions of interest. *Neuroimage*. 2006;31:968−980.
31. Pizzagalli F, Auzias G, Yang Q, et al. The reliability and heritability of cortical folds and their genetic correlations across hemispheres. *Commun Biol*. 2020;3:510.
32. Bowden J, Davey Smith G, Burgess S. Mendelian randomization with invalid instruments: effect estimation and bias detection through Egger regression. *Int J Epidemiol*. 2015;44:512−525.
33. Bowden J, Davey Smith G, Haycock PC, Burgess S. Consistent estimation in mendelian randomization with some invalid instruments using a weighted median estimator. *Genet Epidemiol*. 2016;40:304−314.
34. Siedlinski M, Carnevale L, Xu X, et al. Genetic analyses identify brain structures related to cognitive impairment associated with elevated blood pressure. *Eur Heart J*. 2023;44:2114−2125.
35. Evangelou E, Warren HR, Mosen-Ansorena D, et al. Genetic analysis of over 1 million people identifies 535 new loci associated with blood pressure traits. *Nat Genet*. 2018;50:1412−1425.
36. Binnewies J, Nawijn L, van Tol M-J, et al. Associations between depression, lifestyle and brain structure: a longitudinal MRI study. *Neuroimage*. 2021;231:117834.
37. Chen W, Feng J, Guo J, et al. Obesity causally influencing brain cortical structure: a Mendelian randomization study. *Cereb Cortex*. 2023;33:9409−9416.
38. Yengo L, Sidorenko J, Kemper KE, et al. Meta-analysis of genome-wide association studies for height and body mass index in ∼700000 individuals of European ancestry. *Hum Mol Genet*. 2018;27:3641−3649.
39. Benjamini Y, Hochberg YJ. Controlling the false discovery rate: a practical and powerful approach to multiple testing. *J R Stat Soc Methodol*. 1995;57:289−300.
40. Pierce BL, Ahsan H, Vanderweele TJ. Power and instrument strength requirements for Mendelian randomization studies using multiple genetic variants. *Int J Epidemiol*. 2011;40:740−752.
41. Segarra M, Aburto MR, Cop F, et al. Endothelial Dab1 signaling orchestrates neuro-glia-vessel communication in the central nervous system. *Science*. 2018;361:eaao2861.

42. Liebner S, Dijkhuizen RM, Reiss Y, et al. Functional morphology of the blood-brain barrier in health and disease. *Acta Neuropathol*. 2018;135:311−336.
43. Zhao Z, Nelson AR, Betsholtz C, Zlokovic BV. Establishment and dysfunction of the blood-brain barrier. *Cell*. 2015;163:1064−1078.
44. Kaur C, Foulds WS, Ling EA. Blood-retinal barrier in hypoxic ischaemic conditions: basic concepts, clinical features and management. *Prog Retin Eye Res*. 2008;27:622−647.
45. Huang Y, Wang J, Cai J, et al. Targeted homing of CCR2-overexpressing mesenchymal stromal cells to ischemic brain enhances post-stroke recovery partially through PRDX4-mediated blood-brain barrier preservation. *Theranostics*. 2018;8:5929−5944.
46. Sweeney MD, Sagare AP, Zlokovic BV. Blood-brain barrier breakdown in Alzheimer disease and other neurodegenerative disorders. *Nat Rev Neurol*. 2018;14:133−150.
47. Antonetti DA, Silva PS, Stitt AW. Current understanding of the molecular and cellular pathology of diabetic retinopathy. *Nat Rev Endocrinol*. 2021;17:195−206.
48. Cash A, Theus MH. Mechanisms of blood-brain barrier dysfunction in traumatic brain injury. *Int J Mol Sci*. 2020;21:3344.
49. Wang Y, Rattner A, Zhou Y, et al. Norrin/Frizzled4 signaling in retinal vascular development and blood brain barrier plasticity. *Cell*. 2012;151:1332−1344.
50. Shi H, Koronyo Y, Rentsendorj A, et al. Identification of early pericyte loss and vascular amyloidosis in Alzheimer's disease retina. *Acta Neuropathol*. 2020;139:813−836.
51. Alves JN, Westner BU, Hojlund A, et al. Structural and functional changes in the retina in Parkinson's disease. *J Neurol Neurosurg Psychiatry*. 2023;94:448−456.
52. Friedel EBN, Tebartz van Elst L, Schafer M, et al. Retinal thinning in adults with autism spectrum disorder. *J Autism Dev Disord*. 2022. https://doi.org/10.1007/s10803-022-05882-8.
53. Garcia-Medina JJ, Garcia-Pinero M, Del-Rio-Vellosillo M, et al. Comparison of foveal, macular, and peripapillary intraretinal thicknesses between autism spectrum disorder and neurotypical subjects. *Invest Ophthalmol Vis Sci*. 2017;58:5819−5826.
54. Appaji A, Nagendra B, Chako DM, et al. Retinal vascular abnormalities in schizophrenia and bipolar disorder: a window to the brain. *Bipolar Disord*. 2019;21:634−641.
55. Komatsu H, Onoguchi G, Jerotic S, et al. Retinal layers and associated clinical factors in schizophrenia spectrum disorders: a systematic review and meta-analysis. *Mol Psychiatry*. 2022;27:3592−3616.
56. Igarashi KM. Entorhinal cortex dysfunction in Alzheimer's disease. *Trends Neurosci*. 2023;46:124−136.
57. Yang H, Xu H, Li Q, et al. Study of brain morphology change in Alzheimer's disease and amnestic mild cognitive impairment compared with normal controls. *Gen Psychiatr*. 2019;32:e100005.
58. Greene SJ, Killiany RJ. Subregions of the inferior parietal lobule are affected in the progression to Alzheimer's disease. *Neurobiol Aging*. 2010;31:1304−1311.
59. Guo T, Landau SM, Jagust WJ. Detecting earlier stages of amyloid deposition using PET in cognitively normal elderly adults. *Neurology*. 2020;94:e1512−e1524.
60. Huang C, Wahlund L-O, Svensson L, et al. Cingulate cortex hypoperfusion predicts Alzheimer's disease in mild cognitive impairment. *BMC Neurol*. 2002;2:9.
61. Rolls ET. The cingulate cortex and limbic systems for emotion, action, and memory. *Brain Struct Funct*. 2019;224:3001−3018.
62. Jones BF, Barnes J, Uylings HBM, et al. Differential regional atrophy of the cingulate gyrus in Alzheimer disease: a volumetric MRI study. *Cereb Cortex*. 2006;16:1701−1708.
63. Leech R, Sharp DJ. The role of the posterior cingulate cortex in cognition and disease. *Brain*. 2014;137:12−32.
64. Mitelman SA, Shihabuddin L, Brickman AM, et al. Volume of the cingulate and outcome in schizophrenia. *Schizophr Res*. 2005;72:91−108.
65. Fujiwara H, Hirao K, Namiki C, et al. Anterior cingulate pathology and social cognition in schizophrenia: a study of gray matter, white matter and sulcal morphometry. *Neuroimage*. 2007;36:1236−1245.
66. Lahutsina A, Spaniel F, Mrzilkova J, et al. Morphology of anterior cingulate cortex and its relation to schizophrenia. *J Clin Med*. 2022;12:33.
67. Yamasaki S, Yamasue H, Abe O, et al. Reduced gray matter volume of pars opercularis is associated with impaired social communication in high-functioning autism spectrum disorders. *Biol Psychiatry*. 2010;68:1141−1147.
68. Ye R, Touroutoglou A, Brickhouse M, et al. Topography of cortical thinning in the Lewy body diseases. *Neuroimage Clin*. 2020;26:102196.
69. Van Hoesen GW, Augustinack JC, Dierking J, et al. The parahippocampal gyrus in Alzheimer's disease. Clinical and preclinical neuroanatomical correlates. *Ann N Y Acad Sci*. 2000;911:254−274.
70. Cheung CY-L, Ong YT, Ikram MK, et al. Microvascular network alterations in the retina of patients with Alzheimer's disease. *Alzheimers Dement*. 2014;10:135−142.
71. Georgy L, Lewis JD, Bezgin G, et al. Changes in peri-calcarine cortical thickness in blindsight. *Neuropsychologia*. 2020;143:107463.
72. Conway BR. The organization and operation of inferior temporal cortex. *Annu Rev Vis Sci*. 2018;4:381−402.
73. Abdul-Kareem IA, Sluming V. Heschl gyrus and its included primary auditory cortex: structural MRI studies in healthy and diseased subjects. *J Magn Reson Imaging*. 2008;28:287−299.
74. Henderson D, Bichoutar I, Moxham B, et al. Descriptive and functional anatomy of the Heschl Gyrus: historical review, manual labelling and current perspectives. *Surg Radiol Anat*. 2023;45:337−350.
75. Sun C, Wang JJ, Mackey DA, Wong TY. Retinal vascular caliber: systemic, environmental, and genetic associations. *Surv Ophthalmol*. 2009;54:74−95.
76. Nguyen TT, Wong TY. Retinal vascular manifestations of metabolic disorders. *Trends Endocrinol Metab*. 2006;17:262−268.
77. Wong TY, Scott IU. Clinical practice. Retinal-vein occlusion. *N Engl J Med*. 2010;363:2135−2144.